

2017

# Working-Fluid Selection for Minimized Thermal Resistance in Ultra-Thin Vapor Chambers

G. Patankar

*Purdue University*

J A. Weibel

*Purdue University, jaweibel@purdue.edu*

S V. Garimella

*Purdue University, sureshg@purdue.edu*

Follow this and additional works at: <https://docs.lib.purdue.edu/coolingpubs>

---

Patankar, G.; Weibel, J A.; and Garimella, S V., "Working-Fluid Selection for Minimized Thermal Resistance in Ultra-Thin Vapor Chambers" (2017). *CTRC Research Publications*. Paper 311.

<http://dx.doi.org/10.1016/j.ijheatmasstransfer.2016.09.038>

This document has been made available through Purdue e-Pubs, a service of the Purdue University Libraries. Please contact [epubs@purdue.edu](mailto:epubs@purdue.edu) for additional information.

# Working-fluid selection for minimized thermal resistance in ultra-thin vapor chambers

Gaurav Patankar, Justin A. Weibel, and Suresh V. Garimella\*

*Cooling Technologies Research Center, an NSF I/UCRC  
School of Mechanical Engineering, Purdue University  
585 Purdue Mall, West Lafayette, IN 47907 USA*

## Abstract

The behavior of a vapor chamber is strongly coupled to the thermophysical properties of the working fluid within. It is well known that these properties limit the maximum power (heat load) at which a vapor chamber can operate, due to incidence of the capillary limit. At this limit, the available capillary pressure generated within the wick structure balances the total pressure drop incurred along the path of fluid flow within the wick. A common figure of merit prioritizes working fluids that maximize this capillary-limited operating power. The current work explores working fluid selection for ultra-thin vapor chambers based on a thermal performance objective, rather than for maximized power dissipation capability. A working fluid is sought in this case that provides the minimal thermal resistance while ensuring a capillary limit is not reached at the target operating power. A resistance-network-based model is used to develop a simple analytical relationship for the vapor chamber thermal resistance as a function of the working fluid properties, operating power, and geometry. At small thicknesses, the thermal resistance of vapor chambers becomes governed by the saturation temperature gradient in the vapor core, which is dependent on the thermophysical properties of the working fluid. To satisfy the performance objective, it is shown that the choice of working fluid cannot be based on a single figure of merit containing only fluid properties. Instead, the functional relationship for thermal resistance must be analyzed taking into account all operating and geometric parameters, in addition to the thermophysical fluid properties. Such an approach for choosing the working fluid is developed and demonstrated.

**Keywords:** mobile device thermal management, ultra-thin vapor chamber, heat pipe, working fluid, figure of merit

---

\* Corresponding author: Tel. 765 494 5621 ; [sureshg@purdue.edu](mailto:sureshg@purdue.edu)

## Nomenclature

$a_1, a_2$	constants in $k_{vap}$ relation [-]
$A$	factor $(\frac{\phi^3}{f(1-\phi)^2})$ [-]
$C$	arbitrary constant [m W <sup>-0.5</sup> ]
$d_p$	particle diameter [m]
$f$	factor in Carman-Kozeny relation [-]
$F_s$	factor of safety [-]
$h_{fg}$	specific enthalpy of vaporization [kJ kg <sup>-1</sup> ]
$k_{vap}$	vapor core effective conductance [W K <sup>-1</sup> ]
$k_{wick}$	wick effective conductivity [W m <sup>-1</sup> K <sup>-1</sup> ]
$K$	permeability [m <sup>2</sup> ]
$m$	ratio of particle diameter with effective pore radius ( $d_p/r_{eff}$ ) [-]
$\dot{m}$	mass flow rate [kg s <sup>-1</sup> ]
$M_l$	liquid figure of merit $(\frac{\gamma\rho_l h_{fg}}{\mu_l})$ [W m <sup>-2</sup> ]
$M_{l,min}$	minimum required liquid figure of merit [W m <sup>-2</sup> ]
$M_v$	vapor figure of merit $(\frac{P_v \rho_v h_{fg}^2}{\mu_v R_g T_v^2})$ [W m <sup>-3</sup> K <sup>-1</sup> ]
$n$	number of particle diameters along the wick thickness [-]
$P$	pressure [Pa]
$P_v$	vapor pressure [Pa]
$P_{cap}$	capillary pressure [Pa]

$Q$	power [W]
$r$	radial coordinate [m]
$r_{eff}$	effective pore radius [m]
$R$	radius of vapor chamber [m]
$R_e$	radius of evaporator [m]
$Re$	Reynolds number [-]
$R_g$	gas constant [ $\text{J kg}^{-1} \text{K}^{-1}$ ]
$t$	working thickness [m]
$t_{vap}$	vapor core thickness [m]
$t_{wick}$	wick thickness [m]
$T$	temperature [K]
$u_r$	radial velocity [ $\text{m s}^{-1}$ ]
$U_r$	radial velocity scale [ $\text{m s}^{-1}$ ]
$z$	axial coordinate [m]

***Greek symbols***

$\gamma$	surface tension [ $\text{N m}^{-1}$ ]
$\mu$	dynamic viscosity [ $\text{Pa s}$ ]
$\rho$	density [ $\text{kg m}^{-3}$ ]
$\phi$	porosity [-]

***Subscript***

$l$	liquid phase
$v$	vapor phase
$vap$	vapor core domain

*wick*

wick domain

## 1. Introduction

Portable electronic device platforms such as smartphones and tablets are trending toward thinner, more compact designs with greater embedded functionality (which in turn leads to more waste heat generation from active components). Due to constraints on power consumption and size, it is not practical to use active air cooling methods, or large heat sinks that enhance heat rejection area, to dissipate heat. It is therefore critical to spread heat generated within the device as uniformly as possible over the entire outer skin, where it must be dissipated by natural convection. A vapor chamber passively spreads heat from a localized heat source to a larger heat rejection surface. The sealed chamber contains a working fluid and is lined on its inner surface with a porous wick. Vapor is generated at the evaporator section. The vapor is driven outward and away from the evaporator, and condenses on the inner surface of the opposing wall. The wick passively pumps the condensed liquid back to the evaporator. Ultra-thin vapor chambers offer a viable heat spreading solution in portable electronic device platforms, and can alleviate hot spots on the surface.

A few studies in the literature have focused on the fabrication of ultra-thin vapor chambers to meet this application need. Aoki *et al.* [1] fabricated heat pipes with thicknesses of less than 1 mm using a process that simply flattened traditional cylindrical grooved heat pipes. Ding *et al.* [2] fabricated a titanium-based vapor chamber with a thickness of 0.6 mm, which included a uniform array of microfabricated titanium pillars as the wick structure. Lewis *et al.* [3] fabricated a flexible heat pipe of 0.5 mm thickness made of copper-cladded polyimide, with a copper mesh wick.

The choice of a working fluid is crucial in the design of such vapor chambers. Given the principle of operation of a vapor chamber (a two-phase thermodynamic cycle), the

thermophysical properties of the fluid significantly impact its performance. One conventional ‘figure of merit’ used for guiding the choice of working fluid prioritizes maximizing the operating power. A vapor chamber can operate at a given power only if the capillary pressure available to drive the liquid through the porous wick is larger than the pressure drop; beyond this power level, the vapor chamber will reach the capillary limit and the evaporator will be starved of liquid. This figure of merit is derived by equating the capillary pressure and the pressure drop incurred, which results in a single grouping of thermophysical liquid properties [4] given by

$$M_l = \frac{\gamma \rho_l h_{fg}}{\mu_l} . \quad (1)$$

A higher value for this figure of merit indicates that the vapor chamber can operate at a larger power prior to reaching the capillary limit. A high surface tension yields a higher capillary pressure, while higher density and latent heat reduce the liquid volume flow rate (for a given power input); a lower viscosity leads to a lower pressure drop in the wick. Other less common vapor chamber operational limits include a sonic limit [5] where high vapor velocities lead to choked flow, or an entrainment limit [5] where liquid is entrained into the vapor flowing in the opposite direction by shear forces, starving the evaporator of liquid flow. Along with these phenomenological limits, there are additional practical constraints on working fluid selection. A high fluid vapor pressure at the operating temperature may breach mechanical limits on the pressure that can be supported by the vapor chamber walls. The working fluid also must be chemically compatible with other materials used to construct the vapor chamber.

Recent technology development has focused on vapor chamber designs for high-performance electronics requiring the dissipation of high heat fluxes (over 500 W/cm<sup>2</sup>) [6]. The thermal resistance of such vapor chambers, as well as of more conventional vapor chambers with a

comparatively thick form factor, is dominated by the resistance across the wick at the evaporator. The design of such vapor chambers typically focuses on the evaporator wick, and aims to reduce thermal resistance in the evaporative [5, 6] or boiling regimes [7, 8]. The thermophysical properties of the fluid have a comparatively smaller effect on the thermal resistance in these vapor chamber designs compared to the capillary limit. Fluid selection can therefore be based on the liquid figure of merit alone to maximize the operating power for such thick high-heat-flux dissipating vapor chamber devices.

The thermal resistance of vapor chambers becomes dominated by the temperature gradient in the vapor core as the thickness is reduced. An ultra-thin vapor core induces a high pressure gradient, and hence a high saturation temperature gradient. This thermal resistance is governed by the fluid thermophysical properties. Such a high temperature gradient along the vapor core leads to a high temperature variation along the condenser surface. Patankar *et al.* [11] experimentally observed this variation in temperature along the condenser surface when characterizing the performance of ultra-thin vapor chambers; the vapor chamber resistance changed with operating temperature due to changes in the thermophysical properties with temperature. Yadavalli *et al.* [12] analyzed the performance limitations of a thin heat pipe using a resistance-network-based model. In the limit of low power (where the capillary limit is not of concern), the authors developed a figure of merit based on the thermophysical fluid properties that affect the vapor core thermal resistance, given as

$$M_v = \frac{P_v \rho_v h_{fg}^2}{\mu_v R_g T_v^2}. \quad (2)$$

A higher value for this figure of merit corresponds to a lower thermal resistance in the vapor core.

While these two prevailing figures of merit are useful in the extreme cases where the exclusive concern is either maximizing total heat dissipation power ( $M_I$ ) or minimizing vapor chamber thickness ( $M_v$ ), a more practical design objective is *to select a working fluid that provides the minimal thermal resistance while ensuring that the capillary limit is not reached at the target operating power for a given vapor chamber size*. These figures of merit are also developed using modeling frameworks that intrinsically assume that the vapor chamber design is held constant when comparing across fluids; however, this may not be an appropriate comparison if the design could be tuned to take advantage of favorable characteristics unique to each candidate fluid. For example, the overall thickness may be constrained, but the vapor chamber wick thickness should be free to vary in the design based on the choice of working fluid.

The current work provides guidelines for the process of choosing a working fluid that yields the minimum thermal resistance for ultra-thin vapor chambers, which go beyond the more simplistic existing figures of merit. An analytical expression is developed for the effective resistance of an ultra-thin vapor chamber of axisymmetric geometry. Based on the expression, the significance of the existing individual figures of merit is discussed at the operational extremes. An approach is demonstrated for choosing the working fluid for any operating and geometric parameters, utilizing the complete analytical expression.

## **2. Model**

A working fluid should be chosen to yield the best possible thermal performance, typically characterized in terms of the effective thermal resistance of the vapor chamber. A physics-based

transport model for vapor chamber operation which predicts the effective thermal resistance is hence required to inform working fluid selection. To develop a standard practice for working fluid selection, we base the selection process in this work on a conventional thermal resistance network modeling approach [13]. This modeling approach divides the vapor chamber domain into a network of one-dimensional thermal resistances corresponding to conduction in the wall and wick, evaporation/condensation at the interfaces, and temperature drop in the vapor core. The performance of an ‘ultra-thin’ vapor chamber having negligible thermal resistance across the thickness of the wall and wick can be simply represented by the vapor core effective conductance, defined as

$$k_{vap} = \frac{Q}{\Delta T_{vap}}. \quad (3)$$

where  $\Delta T_{vap}$  is the total saturation temperature change due to the pressure drop in the vapor core.

The geometry of the vapor chamber selected for demonstration of this fluid selection strategy is illustrated in Figure 3; this is representative of a typical internal layout in vapor chambers. The vapor chamber is disc-shaped with radius  $R$ . The evaporator is a circle of radius  $R_e$  at the center of one face of the vapor chamber, with a power input  $Q$ . The entire opposing face acts as the condenser. The vapor chamber has walls of constant thickness. There is a uniform layer of wick (thickness  $t_{wick}$ ) on internal surfaces of the chamber. A working thickness ( $t$ ) is defined as the total thickness of the vapor core ( $t_{vap}$ ) plus the two wick layers on each side ( $2 \times t_{wick}$ ). The total working thickness is assumed to have a constant value (based on space constraints), but the relative thicknesses occupied by the wick and vapor core are allowed to vary.

The model is used to assess the effect of fluid properties on vapor chamber performance in two steps. (1) As a design premise, the wick thickness should be minimized to enable the largest vapor core thickness possible; a required minimum wick thickness is computed based on the capillary limit at power  $Q$  for each fluid. (2) The second step is computing the vapor core effective conductance for each respective vapor core thickness, and use it to compare and assess fluids. The primary objective of the current modeling approach is to obtain a simple analytical relationship (rather than a high-fidelity prediction) for the vapor core effective conductance that is a function of the fluid properties, vapor chamber geometry, and operating power. The same fluid selection approach presented here could be applied using alternative, high-fidelity model frameworks [14, 15].

### *2.1 Design for minimized wick thickness*

For a vapor chamber to operate, the capillary pressure driving the fluid flow must be larger than the pressure drop. To design for the minimum required wick thickness, the capillary pressure is equated to the pressure drop in the wick (*i.e.*, capillary limit at this minimum thickness). The pressure drop in the vapor core, although larger than conventional ‘thick’ vapor chambers, is still typically significantly less than the pressure drop in the wick for ultra-thin vapor chambers, and therefore is not considered. The capillary pressure in the wick is defined by

$$P_{cap} = \frac{2\gamma}{r_{eff}}; r_{eff} = md_p, \quad (4)$$

where the effective pore radius ( $r_{eff}$ ) is proportional to the particle diameter of the wick ( $d_p$ ) with a proportionality constant of  $m$ . The pressure drop in the wick is computed using Darcy’s law for

one-dimensional radial flow. This assumes that all of the pressure gradient in the porous wick structure is attributed to viscous drag based on the relation given by

$$\frac{dP_{wick}}{dr} = -\frac{\mu_l}{K} u_{r,wick}(r); u_{r,wick}(r) = \frac{\dot{m}_{wick}(r)}{\rho_l 2\pi r t_{wick}}. \quad (5)$$

The permeability of the wick can be expressed using the Carman-Kozeny relation, given by

$$K = \frac{d_p^2 \phi^3}{f(1-\phi)^2} = Ad_p^2, \quad (6)$$

where  $f$  is an empirical factor depending on the wick morphology; the term  $A$  is introduced to simplify presentation of this expression in subsequent equations.

In the condenser-side wick, the outward liquid mass flow is supplied by condensation at the wick-vapor interface. We assume that the rate of condensation is uniform across the entire interface (constant mass flux across the interface) to obtain a simplified analytical expression for the mass flow rate:

$$\dot{m}_{wick}(r) = \frac{Q}{h_{fg}} \left( \frac{r}{R} \right)^2. \quad (7)$$

In the evaporator-side wick, we assume mass flow is reduced by uniform evaporation over the heat input area ( $0 < r < R_e$ ). Hence, the mass flow rate is expressed as:

$$\dot{m}_{wick}(r) = -\frac{Q}{h_{fg}} \text{ for } r > R_e$$

$$\dot{m}_{wick}(r) = -\left( \frac{Q}{h_{fg}} - \frac{Q}{h_{fg}} \left( 1 - \left( \frac{r}{R_e} \right)^2 \right) \right) \text{ for } r < R_e \quad (8)$$

Substituting the expressions for mass flow rate in Eqs. (7) and (8) into Eq. (5) and integrating yields the total pressure drop in the wick:

$$\Delta P_{wick} = \frac{\mu_l Q}{2\pi h_{fg} \rho_l t_{wick} A d_p^2} \left( \ln \left( \frac{R}{R_e} \right) + \frac{5}{8} \right). \quad (9)$$

The particle diameter is defined as a fixed fraction of the wick thickness ( $d_p = t_{wick} / n$ ). A factor of safety  $F_s$  is introduced for the wick pressure drop, to avoid the certain failure if the capillary limit were reached:

$$P_{cap} = F_s \times \Delta P_{wick}. \quad (10)$$

This results in the following relation for minimum wick thickness

$$t_{wick} = \frac{1}{2} a_1 \left( \frac{Q}{M_l} \right)^{0.5}; \quad M_l = \frac{\rho_l \gamma h_{fg}}{\mu_l}; \quad a_1 = 2 \left( \frac{nm F_s}{4\pi A} \left( \ln \left( \frac{R}{R_e} \right) + \frac{5}{8} \right) \right)^{0.5}. \quad (11)$$

## 2.2 Expression for vapor core effective conductance as a function of $M_v$

The temperature gradient in the vapor core is due to the saturation pressure gradient. The pressure gradient is computed using the steady-state fluid momentum transfer equation (cylindrical coordinates) in the radial direction. The following simplifying assumptions are used:

(1) for  $t_{vap} \ll R$ , momentum diffusion predominantly occurs in the  $z$ -direction, (2) for

$Re \left( \frac{t_{vap}}{R} \right)^2 \ll 1$  where  $Re = \frac{\rho_v U_r R}{\mu_v}$ , convection is negligible compared to diffusion in the  $z$ -

direction. The resulting equation is

$$\frac{dP_{vap}}{dr} = \mu \frac{d^2 u_{r,vap}}{dz_{vap}^2}. \quad (12)$$

Integrating twice along  $z$  gives the velocity profile

$$u_{r,vap} = -\frac{t_{vap}^2}{8\mu} \frac{dP_{vap}}{dr} \left( 1 - \frac{4z_{vap}^2}{t_{vap}^2} \right). \quad (13)$$

The mass flow rate in the vapor core is given by  $\dot{m}_{vap}(r) = \int_{-t_{vap}/2}^{t_{vap}/2} \rho_v u_{r,vap} 2\pi r dz_{vap}$ . Combining with Eq. (13) yields

$$\frac{dP_{vap}}{dr} = -\frac{6\mu_v \dot{m}_{vap}(r)}{\pi t_{vap}^3 r \rho_v}. \quad (14)$$

The vapor mass flow rate at any radial location is the difference between evaporation mass rate and condensation mass rate:

$$\begin{aligned} \dot{m}_{vap}(r) &= \frac{Q}{h_{fg}} \left( \frac{r^2}{R_e^2} - \frac{r^2}{R^2} \right) \quad \text{for } r < R_e \\ \dot{m}_{vap}(r) &= \frac{Q}{h_{fg}} \left( 1 - \frac{r^2}{R^2} \right) \quad \text{for } r > R_e \end{aligned} \quad (15)$$

Substituting Eq. (15) into Eq. (14) and integrating over  $r$  gives the pressure drop in the vapor core as

$$\Delta P_{vap} = \frac{6\mu_v Q}{\pi t_{vap}^3 \rho_v h_{fg}} \ln \left( \frac{R}{R_e} \right). \quad (16)$$

The temperature difference in the vapor-core is obtained using the Clausius-Clapeyron relation

$$\Delta T_{vap} = \frac{R_g T_v^2}{P_v h_{fg}} \Delta P_{vap} = \frac{6R_g T_v^2 \mu_v Q}{P_v \pi t_{vap}^3 \rho_v h_{fg}^2} \ln \left( \frac{R}{R_e} \right) \quad (17)$$

where  $P_v$  and  $T_v$  are taken as the average vapor pressure and temperature. The ultimate performance of the vapor chamber is expressed by the effective vapor core conductance,

$$k_{vap} = \frac{Q}{\Delta T_{vap}} = a_2 M_v t_{vap}^3; \quad M_v = \frac{P_v \rho_v h_{fg}^2}{R_g T_v^2 \mu_v}; \quad a_2 = \frac{\pi}{6 \ln \left( \frac{R}{R_e} \right)}. \quad (18)$$

To obtain an expression based on the desired design parameter of the constraining working thickness  $t$ , we substitute  $t_{vap} = t - 2t_{wick}$  into Eq. (11) to get:

$$k_{vap} = a_2 M_v \left( t - a_1 \left( \frac{Q}{M_l} \right)^{0.5} \right)^3. \quad (19)$$

This model assumes that the vapor chamber thermal resistance is dominated by the vapor core resistance. The assumption is valid when the vapor core resistance is larger than all other primary resistances (*viz.*, the diffusive thermal resistance in the wick and the solid wall and the resistance due to phase change). A simple check of the model validity is provided by ensuring that the vapor-core conductance is significantly less than the evaporator wick conductance, according to

$$. a_2 M_v \left( t - a_1 \left( \frac{Q}{M_l} \right)^{0.5} \right)^3 \ll \frac{k_{wick} \pi R_e^2}{\frac{1}{2} a_1 \left( \frac{Q}{M_l} \right)^{0.5}} \quad (20)$$

### 3. Results

The model developed above indicates that the vapor core effective conductance (Eq. (19)) increases with an increase in either of the conventional figures of merit that contain both liquid properties ( $M_l$ ) and vapor properties ( $M_v$ ). A candidate working fluid with higher values of both  $M_l$  and  $M_v$  can be deemed preferable without computing the vapor-core effective conductance. However, when comparing two fluids where the value of  $M_l$  is higher for one fluid but  $M_v$  is higher for the other (or *vice versa*), the appropriate choice can only be made by computing the vapor core effective conductance using Eq. (19). Thus, while figures of merit containing only fluid properties ( $M_l$  and  $M_v$ ) are useful indicators in some instances, a generalized model for the vapor chamber thermal resistance is required for choosing the working fluid, as demonstrated below.

The vapor core effective conductance depends not only on the fluid property figures of merit, but also on different vapor chamber geometric parameters and operating conditions. This study analyzes the effects of three key parameters, namely operating power, working thickness, and operating temperature, on the vapor core conductance (and hence the choice of working fluid).

### 3.1 Effect of operating power and working thickness on the choice of working fluid

The operating power has a significant effect on fluid choice. Consider the vapor core conductance in the limit of a very low operating power. Eq. (19) becomes

$$\{Q \rightarrow 0\} \Rightarrow \left\{ a_1 \left( \frac{Q}{M_l} \right)^{0.5} \rightarrow 0 \right\} \Rightarrow \{k_{vap} \rightarrow a_2 M_v t^3\}. \quad (21)$$

At a low operating power, a fluid with a high value of  $M_v$  is preferred; the value of  $M_l$  is less relevant. On the other hand, a high value of operating power implies

$$\left\{ t_{wick} = a_1 \left( \frac{Q}{M_l} \right)^{0.5} \right\} \rightarrow t, \quad (22)$$

*i.e.*, the wick thickness will approach the limit where it must occupy the entire working thickness in order to convey liquid at the high operating power. Thus, to keep the value of wick thickness below the available working thickness, a working fluid with a high value of  $M_l$  is critical; the value of  $M_v$  is less relevant.

This influence of operating power is illustrated using three example fluids: water, acetone, and pentane. Figure 4 shows a contour map of the vapor core conductance as a function of  $M_l$  (horizontal axis) and  $M_v$  (vertical axis); the different panels consider evaporator input powers of 0.25 W, 1 W, and 3 W. The vapor core effective conductances of the fluids are marked on the contours. Pentane has the highest  $M_v$  and lowest  $M_l$ , water has the highest  $M_l$  and lowest  $M_v$ , and acetone has intermediate values. The thermophysical properties of the fluids are computed using the REFPROP database [17].

At the lowest operating power of 0.25 W, the contour lines are the most parallel to the  $M_l$  axis, among the three cases considered. This is consistent with the conclusion drawn with Eq. (21) that the fluid choice is dominated by the value of  $M_v$  at low powers. In this example, pentane has the highest vapor core effective conductance, and would be the best choice of working fluid. At the intermediate operating power of 1 W, the contour lines are more angled from the horizontal axis (compared to the 0.25 W case) and  $M_l$  has a higher influence on the vapor core effective conductance. Thus, pentane is heavily penalized for its low  $M_l$ , and acetone is the best choice. At this power, the contour plot includes a vertical line marked  $M_{l,min}$ . For values of  $M_l$  lower than this limit, the minimum wick thickness required to avoid a capillary limit would exceed the available working thickness, and such a fluid is unviable. At the highest power

of 3 W, the relative importance of  $M_l$  is even greater. The requirement imposed by  $M_{l,min}$  excludes pentane and acetone as candidate working fluids. Water, which has the highest value of  $M_l$ , is the best choice despite having the lowest value of  $M_v$ .

Besides operating power, the working thickness also affects the choice of working fluid. Guidelines for choosing the best-performing working fluid for an ultra-thin vapor chamber can be represented on a map of the operating power ( $Q$ ) and working thickness ( $t$ ); this  $Q$ - $t$  space can then be divided into regions where particular fluids have the best performance. This is illustrated in Figure 5a for a map generated using the example set of fluids (with corresponding values of  $M_l$  and  $M_v$ ) shown in Table 1. To generate this fluid selection map, the value of the vapor core effective conductance for each fluid is computed throughout the  $Q$ - $t$  space; regions on the map are colored according to the fluid that has the highest vapor core conductance. The map in Figure 5a was generated for a grid of 60×60 points over the range of operating powers and working thicknesses shown. A fluid selection tool with a graphical user interface was developed using the commercial software MATLAB [16] to generate such  $Q$ - $t$  space maps as a function of user-defined vapor chamber geometric and operating parameters, and is included as Supplementary Data.

The effect of power and working thickness on fluid choice is apparent in this map (Figure 5a). With increasing power, the preferred fluid shifts from one with high  $M_v$  (*e.g.*, pentane) to a fluid with high  $M_l$  (*e.g.*, water); with increasing thickness, the preferred fluid shifts from high  $M_l$  to high  $M_v$ . The map includes a region with high powers and low thicknesses which does not map to a viable working fluid; in this region marked in white, none of the candidate fluids included in the analysis have a sufficiently high  $M_l$  to ensure a wick thickness less than the available working thickness (*i.e.*, in this region,  $M_l < M_{l,min}$  for all candidate fluids).

Note the critical transition lines separating the best-fluid regions in Figure 5. Consider loci in the  $Q$ - $t$  space defined by  $t = C \cdot Q^{0.5}$ , where  $C$  is an arbitrary constant. Substituting in Eq. (19) yields

$$k_{vap} = a_2 M_v \left( C - a_1 \left( \frac{1}{M_l} \right)^{0.5} \right)^3 Q^{1.5}. \quad (23)$$

In this expression, the operating power becomes a standalone multiplier. Thus, the vapor core effective conductance for all the fluids is changed by the same factor related to operating power, and the relative performance between different fluids is unchanged on these loci. This is illustrated in Figure 5a where one example locus with  $C = 100 \mu\text{m W}^{-0.5}$  is shown as a dashed line on which all fluids considered can be ranked by their performance relative to the best fluid; the values in the inset box of Figure 5a provide the vapor conductances weighted against that of acetone for this locus. Transition lines on the  $Q$ - $t$  map are always defined by loci of this functional form at different values of  $C$ .

### 3.2 Effect of operating temperature on the choice of working fluid

The temperature-dependence of the thermophysical fluid properties affects the choice of working fluid that would yield the best performance. For computing fluid properties, the operating temperature can be defined as the area-weighted average temperature on the surface of the condenser because the temperature difference across the thickness of the vapor chamber is minimal. The effect of operating temperature on working fluid choice is illustrated in Figure 5, where the  $Q$ - $t$  maps at temperatures of 325 K, 350 K, and 375 K are shown, generated for the fluids shown in Table 1. The appearance of the map changes based on the temperature-dependent thermophysical properties of each fluid. The operating temperature determines the saturation

pressure of the fluid in the vapor core. It is critical to note that the walls of the vapor chamber must support the pressure difference between the vapor core and ambient, and mechanical design considerations may exclude some working fluids. For example, in the maps shown in Figure 5, fluids which have a vapor pressure higher than an arbitrary limit of 3 atm are shown cross-hatched.

#### 4. Conclusion

This work investigated the effects of the thermophysical properties of working fluids on the performance of ultra-thin vapor chambers. At these form factors, the vapor chamber thermal resistance is dominated by the fluid flow in the vapor core. Based on a design target of minimizing thermal resistance, a simplified analytical relationship is proposed between the vapor core thermal conductance and two fluid figures of merit ( $M_l$  representing liquid properties and  $M_v$  representing vapor properties). A methodology for selecting between working fluids for a given set of ultra-thin vapor chamber geometric and operating parameters was developed. The primary conclusions from this study of the effects of important operating conditions and parameters on the choice of the working fluid are:

- 1) Vapor chambers operating at a relatively high power require a fluid with higher  $M_l$  to prevent the required wick thickness from occupying the entire vapor space; at lower powers, a fluid with high  $M_v$  is preferred, with a tradeoff between these prioritizations in the intermediate power range;

- 2) With decreasing vapor chamber thickness, the preference changes from a fluid with high  $M_v$  to one with high  $M_l$ ; at the lowest thicknesses, a high  $M_l$  becomes a requirement so that the wick does not occupy the entire thickness available; and
- 3) The unique temperature-dependence of thermophysical properties for each fluid govern fluid selection; caution must be exercised to ensure a reasonable vapor pressure at which the structural integrity of the vapor chamber is not compromised.

## Appendix A. Supplementary Data

Supplementary data associated with this article can be found in the online version.

## Acknowledgement

The authors thank Intel Corporation, specifically Program Director Mondira Pant (Intel Labs, University Collaborative Research) and Project Mentor Mark MacDonald, for their support of this work as part of the Intel Strategic Research Alliance (ISRA) on platform thermal cooling solutions.

## References

- [1] H. Aoki, N. Shioya, M. Ikeda, and Y. Kimura, “Development of ultra thin plate-type heat pipe with less than 1 mm thickness,” in 26th Annual IEEE Semiconductor Thermal Measurement and Management Symposium (SEMI-THERM), pp. 217–222, 2010.
- [2] C. Ding, G. Soni, P. Bozorgi, B. D. Piorek, C. D. Meinhart, and N. C. MacDonald, “A flat heat pipe architecture based on nanostructured titania,” *Journal of Microelectromechanical Systems*, vol. 19, no. 4, pp. 878–884, 2010.
- [3] R. Lewis, S. Xu, L. Liew, C. Coolidge, R. Yang, and Y.C. Lee, “Thin flexible thermal ground planes: fabrication and scaling characterization,” *Journal of Microelectromechanical Systems*, vol. 24, no. 6, pp. 2040–2048, 2015.
- [4] P. D. Dunn and D. A. Reay, “The heat pipe,” *Physics in Technology*, vol. 4, no. 3, p. 187, 1973.

- [5] P. D. Dunn and D. A. Reay, *Heat Pipes*, 4th ed. Oxford, England: Elsevier Science, 1994.
- [6] J. A. Weibel and S. V. Garimella, “Recent advances in vapor chamber transport characterization for high-heat-flux applications,” in *Advances in Heat Transfer*, vol. 45, pp. 209–301, 2013.
- [7] J. A. Weibel and S. V. Garimella, “Visualization of vapor formation regimes during capillary-fed boiling in sintered-powder heat pipe wicks,” *International Journal of Heat and Mass Transfer*, vol. 55, no. 13–14, pp. 3498–3510, 2012.
- [8] T. Semenic and I. Catton, “Experimental study of biporous wicks for high heat flux applications,” *International Journal of Heat and Mass Transfer*, vol. 52, no. 21–22, pp. 5113–5121, 2009.
- [9] R. Ranjan, S. V. Garimella, J. Y. Murthy, and K. Yazawa, “Assessment of nanostructured capillary wicks for passive two-phase heat transport,” *Nanoscale Microscale Thermophysical Engineering*, vol. 15, no. 3, pp. 179–194, 2011.
- [10] Y. S. Ju, M. Kaviany, Y. Nam, S. Sharratt, G. S. Hwang, I. Catton, E. Fleming, and P. Dussinger, “Planar vapor chamber with hybrid evaporator wicks for the thermal management of high-heat-flux and high-power optoelectronic devices,” *International Journal of Heat and Mass Transfer*, vol. 60, pp. 163–169, 2013.
- [11] G. Patankar, S. Mancin, J. A. Weibel, S. V. Garimella, and M. A. MacDonald, “A method for thermal performance characterization of ultrathin vapor chambers cooled by natural convection,” *Journal of Electronics Packaging*, vol. 138, no. 1, pp. 010903, 2016.
- [12] Y. Yadavalli, J. A. Weibel, and S. V. Garimella, “Performance-governing transport mechanisms for heat pipes at ultrathin form factors,” *IEEE Transactions on Components, Packaging and Manufacturing Technology*, vol. 5, no. 11, pp. 1618–1627, 2015.
- [13] R. S. Prasher, “A simplified conduction based modeling scheme for design sensitivity study of thermal solution utilizing heat pipe and vapor chamber technology,” *Journal of Electronics Packaging*, vol. 125, no. 3, pp. 378–385, 2003.
- [14] R. Ranjan, J. Y. Murthy, S. V. Garimella, and U. Vadakkan, “A numerical model for transport in flat heat pipes considering wick microstructure effects,” *International Journal of Heat and Mass Transfer*, vol. 54, no. 1–3, pp. 153–168, 2010.
- [15] B. Xiao and A. Faghri, “A three-dimensional thermal-fluid analysis of flat heat pipes,” *International Journal of Heat and Mass Transfer*, vol. 51, no. 11–12, pp. 3113–3126, 2008.
- [16] *MATLAB 2012a*. Natick, Massachusetts, United States: The MathWorks, Inc.
- [17] E. W. Lemmon, M. L. Huber, and M. O. McLinden, *NIST Standard Reference Database 23: Reference Fluid Thermodynamic and Transport Properties-REFPROP, Version 9.1, National Institute of Standards and Technology, Standard Reference Data Program*. Gaithersburg, 2013.

## List of Tables

Table 1. Fluid property figures of merit for six fluids at  $T_v = 325$  K.

## List of Figures

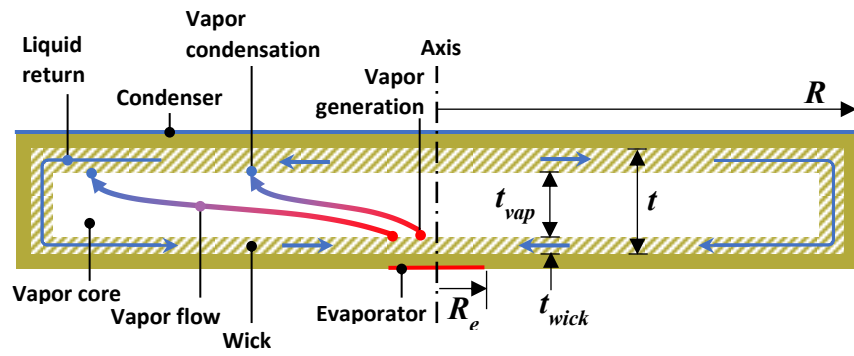
Figure 1: Schematic diagram of the operation of a vapor chamber.

Figure 1: Contours of effective vapor core conductance as a function of the liquid and vapor figures of merit for operating powers of (a) 0.25 W, (b) 1 W, and (c) 3 W.  $R = 45$  mm,  $R_e = 5$  mm,  $t = 100$   $\mu$ m,  $n = 3$ ,  $F_s = 2$ ; the wick is a sintered copper ( $m = 0.21$ ,  $f = 150$ ) with 60 % porosity; thermophysical properties at 325 K.

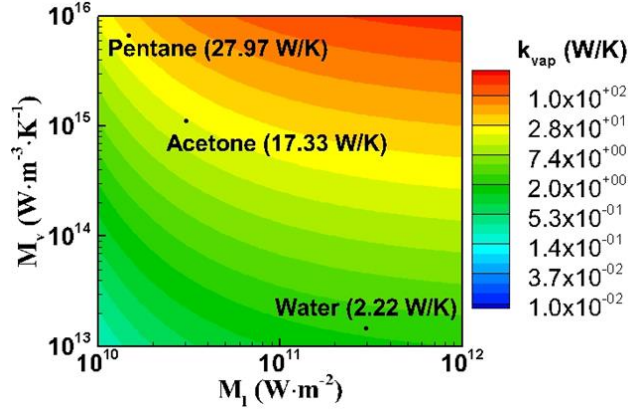
Figure 2: Plots showing the best working fluids in the power–working-thickness space. Properties are calculated at (a)  $T_v = 325$  K, (b)  $T_v = 350$  K, and (c)  $T_v = 375$  K.  $R = 45$  mm,  $R_e = 5$  mm,  $n = 3$ ,  $F_s = 2$ ; the wick is a sintered copper ( $m = 0.21$ ,  $f = 150$ ) with 60 % porosity.

**Table 1. Fluid property figures of merit for six fluids at  $T_v = 325$  K.**

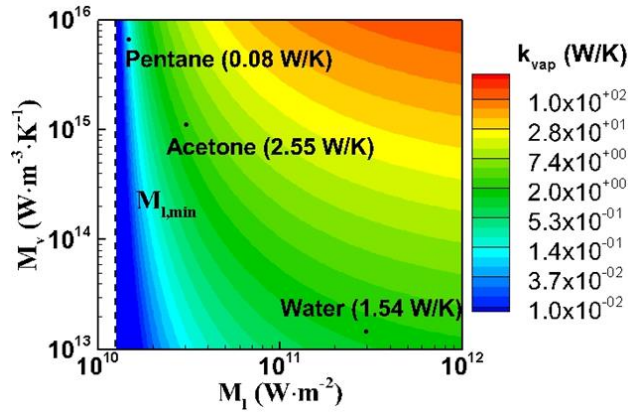
	$M_l$ (W/m <sup>2</sup> )	$M_v$ (W/m <sup>3</sup> K)
Acetone	$3.06 \times 10^{10}$	$23.2 \times 10^{13}$
Methanol	$4.52 \times 10^{10}$	$5.99 \times 10^{13}$
Water	$30.0 \times 10^{10}$	$1.29 \times 10^{13}$
Pentane	$1.47 \times 10^{10}$	$75.6 \times 10^{13}$
Ethanol	$1.87 \times 10^{10}$	$7.31 \times 10^{13}$
R141b	$1.22 \times 10^{10}$	$73.0 \times 10^{13}$



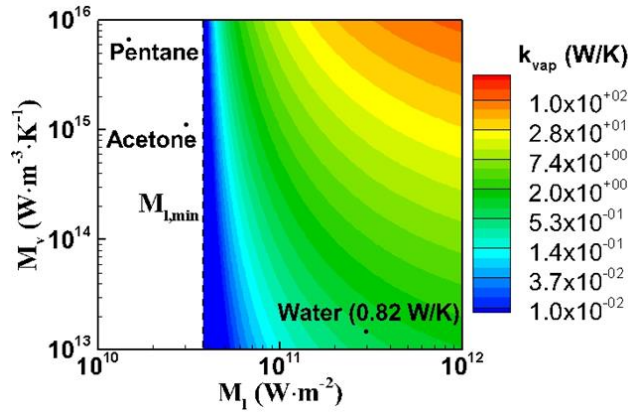
**Figure 3. Schematic diagram of the operation of a vapor chamber.**



(a)  $Q = 0.25$  W

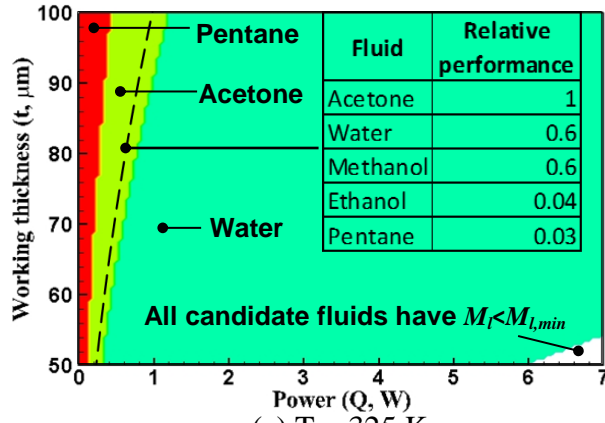


(b)  $Q = 1$  W

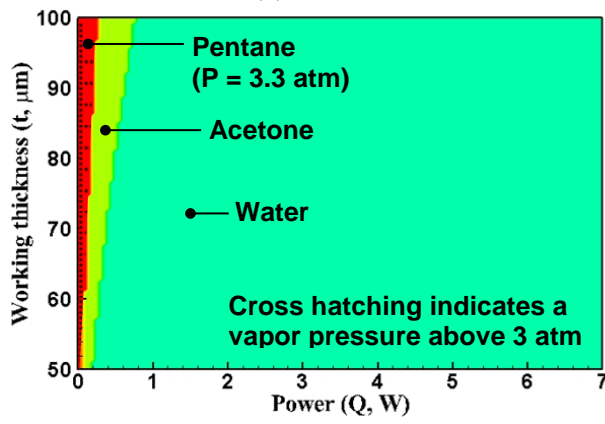


(c)  $Q = 3$  W

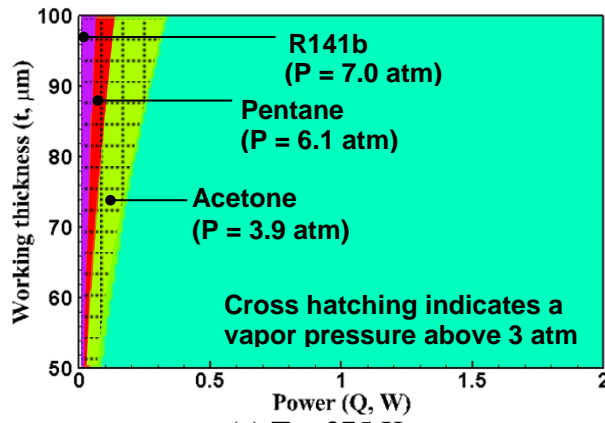
**Figure 4. Contours of effective vapor core conductance as a function of the liquid and vapor figures of merit for operating powers of (a) 0.25 W, (b) 1 W, and (c) 3 W.  $R = 45$  mm,  $R_e = 5$  mm,  $t = 100$   $\mu\text{m}$ ,  $n = 3$ ,  $F_s = 2$ ; the wick is sintered copper ( $m = 0.21$ ,  $f = 150$ ) with 60% porosity; thermophysical properties evaluated at 325 K.**



(a)  $T = 325$  K



(b)  $T = 350$  K



(c)  $T = 375$  K

**Figure 5. Plots showing the best working fluids in the power-working thickness space. Properties are calculated at (a)  $T_v = 325$  K, (b)  $T_v = 350$  K, and (c)  $T_v = 375$  K.  $R = 45$  mm,  $R_e = 5$  mm,  $n = 3$ ,  $F_s = 2$ ; the wick is sintered copper ( $m = 0.21$ ,  $f = 150$ ) with 60% porosity.**